

Dynamical Downscaling Simulation and Future Projection of Extreme Precipitation Activities in Taiwan during the Mei-Yu Seasons

Wan-Ru HUANG, Po-Han HUANG, Ya-Hui CHANG

Department of Earth Sciences, National Taiwan Normal University, Taiwan

Chao-Tzuen CHENG

National Sciences and Technology Center for Disaster Reduction, Taiwan

Huang-Hsiung HSU, Chia-Ying TU

Research Center for Environmental Changes, Academia Sinica, Taiwan

and

Akio KITOH

Japan Meteorological Business Support Center, Tsukuba, Japan

(Manuscript received 4 August 2018, in final form 21 December 2018)

Abstract

By using the Weather Research and Forecasting (denoted as WRF) model driven by two super-high-resolution global models, High Resolution Atmospheric Model (denoted as HiRAM) and Meteorological Research Institute Atmospheric General Circulation Model (denoted as MRI), this study investigates the dynamical downscaling simulation and projection of extreme precipitation activities (including intensity and frequency) in Taiwan during the Mei-Yu seasons (May and June). The analyses focus on two time period simulations: the present-day (1979–2003, historical run) and the future (2075–2099, RCP8.5 scenario). For the present-day simulation, our results show that the bias of HiRAM and MRI in simulating the extreme precipitation activities over Taiwan can be reduced after dynamical downscaling by using the WRF model. For the future projections, both the dynamical downscaling models (i.e., HiRAM-WRF and MRI-WRF) project that extreme precipitation will become more frequent and more intense over western Taiwan but less frequent and less intense over eastern Taiwan. The east-west contrast in the projected changes in extreme precipitation in Taiwan are found to be a local response to the enhancement of southwesterly monsoonal flow over the coastal regions of South China, which leads to an increase in water vapor convergence over the windward side (i.e., western Taiwan) and a decrease in water vapor convergence over the leeward side (i.e., eastern Taiwan). Further examinations of the significance of the projected changes in extreme precipitation that affect the agriculture regions of Taiwan show that the southwestern agriculture regions will be affected by extreme precipitation events more frequently and more intensely than the other subregions. This finding highlights the importance of examining regional differences in the projected changes in extreme precipitation over the complex terrain of East Asia.

Corresponding author: Wan-Ru Huang, Department of Earth Sciences, National Taiwan Normal University, No. 88, Sec. 4, Tingchou Rd., Wenshan District, Taipei 11677, Taiwan R.O.C.

E-mail: wrhuang@ntnu.edu.tw

J-stage Advance Published Date: 10 January 2019



Keywords dynamical downscaling; extreme precipitation; future projection; East Asia

Citation Huang, W.-R., P.-H. Huang, Y.-H. Chang, C.-T. Cheng, H.-H. Hsu, C.-Y. Tu, and A. Kitoh, 2019: Dynamical downscaling simulation and future projection of extreme precipitation activities in Taiwan during the Mei-Yu seasons. *J. Meteor. Soc. Japan*, **97**, 481–499, doi:10.2151/jmsj.2019-028.

1. Introduction

Extreme precipitation has always been a crucial research subject in many countries (e.g., Endo et al. 2009; Agel et al. 2015; Herman and Schumacher 2016; Loriaux et al. 2017). In Taiwan, long-term climatic statistics show that the Mei-Yu season (May and June, or MJ) is one of the major precipitation periods, and approximately 26.3 % of annual precipitation falls during this period (estimated from Fig. 1 of Chen et al. 2004). Although the Mei-Yu season precipitation can provide the water supply for people's livelihoods in Taiwan, it is common to see extreme precipitation events during this period bring disastrous floods and result in economic losses to agriculture. For example, heavy rainfall induced by the Mei-Yu front system from June 2 to June 4, 2017 caused significant damage in Taiwan. Approximately 6,000 hectares of cropland were destroyed, and the economic losses from this natural disaster reached approximately 9 million (U.S. dollars) according to the Council of Agriculture, Executive Yuan in Taiwan. Extensive studies examining the observational data have found that Mei-Yu season extreme precipitation in Taiwan is mostly attributed to the frontal types of precipitation events (including the rainstorms embedded in the frontal system) (e.g., Chen et al. 1989; Chen and Chen 2003; Yeh and Chen 2004; Chen et al. 2011; Wu et al. 2016). Huang and Chen (2015) further noted that the occurrence frequency of frontal precipitation in Taiwan declined (a negative trend) during the Mei-Yu seasons of 1982–2012, which was due to the changes in the East-Asian monsoonal circulation over the past several decades. It is likely that future changes in the East-Asian monsoonal circulation might also play an important role in affecting the Mei-Yu season extreme precipitation activities in Taiwan.

Many studies have compared the present-day simulation and the future projection of extreme precipitation over various countries by using global models to assess future climate changes (e.g., Walsh et al. 2008; Dulière et al. 2011; Shi and Durran 2015; Suzuki et al. 2015; Park et al. 2016). According to the Intergovernmental Panel on Climate Change (IPCC)

reports (IPCC 2013), most global models project that extreme precipitation is very likely to become more intense and more frequent over most of the mid-latitude land masses and wet tropical regions. However, it is well-known that most global models cannot capture the regional precipitation features over areas with complex terrains well (Huang and Wang 2017). Therefore, more studies tend to assess the future changes in precipitation in Taiwan by using dynamical downscaling methods (i.e., using the outputs of global models to drive a higher-resolution regional model) (e.g., Huang et al. 2016a, b, c). For example, Huang et al. (2016a, b) used Weather Research and Forecasting (WRF) driven by two super-high-resolution global models and noted that the dynamical downscaling approach adds valuable information in the present-day simulation of diurnal precipitation over Taiwan and nearby regions (including South China and Luzon). Huang et al. (2016a, b) and others (e.g., Huang and Wang 2017) showed that most global models have problems capturing the right timing of the appearance of the diurnal precipitation maximum in Taiwan. Such a bias can be reduced using the WRF dynamical downscaling simulation (Huang et al. 2016a, b). As inferred from these documented studies, the use of a WRF dynamical downscaling approach might be a good method to reduce the bias of global models in simulating the Mei-Yu season extreme precipitation activities over Taiwan. This issue has not been examined by Huang et al. (2016a, b) or other studies, and it is examined herein.

The main objectives of this study are as follows: (1) to clarify whether the WRF dynamical downscaling approach can add valuable information when simulating the Mei-Yu season extreme precipitation activities (including intensity and frequency) in Taiwan; (2) to clarify whether the projected changes in the Mei-Yu season extreme precipitation activities in Taiwan are location dependent; and (3) to clarify whether the findings of issues (1) and (2) are dependent on the models. The analyses were particularly focused on the projected changes in extreme precipitation activities over agricultural regions because it can provide useful information to the local government when establishing

long-term disastrous prevention policies. Detailed information on the models, the observational data, and the analysis methods are introduced in Section 2. Comparisons of the abilities of the models to simulate the extreme precipitation activities in Taiwan during the present-day (1979–2003, under the historical run) are presented in Section 3. The projected changes, which are defined as the difference between the future projection at the end of the 21st century (2075–2099, under the RCP8.5 scenario) and the present-day simulation, are documented in Section 4. A discussion of the possible causes of the projected changes in the extreme precipitation activities in Taiwan is given in Section 5. A concluding remark is provided in Section 6.

2. Models, observations, and methodology

2.1 Models

Throughout this study, the analyses are based on two time period simulations at the present-day (1979–2003, under the historical run) and at the end of the 21st century (2075–2099, under the RCP8.5 scenario). Here the output from two super-high-resolution global models are adopted to drive the regional model in higher spatial resolution (i.e. dynamical downscaling models). The first global model we used is the High Resolution Atmospheric Model (HiRAM), which has a horizontal resolution of approximately 25 km and originated from the Geophysical Fluid Dynamics Laboratory (GFDL) Atmospheric Model version 2.1 (Zhao et al. 2009). The second global model we used is the Meteorological Research Institute Atmospheric General Circulation Model version 3.2 (MRI-AGCM 3.2; hereafter MRI), which has a horizontal resolution of approximately 20 km and was jointly developed by the Japan Meteorological Agency and the Meteorological Research Institute (Mizuta et al. 2012). The dynamical downscaling experiments, which have a 5-km horizontal resolution, are conducted using the WRF model version 3.5.1 (Skamarock et al. 2008) driven by HiRAM and MRI. Hereafter, WRF driven by HiRAM and MRI are denoted as HiRAM-WRF and MRI-WRF, respectively.

Figure 1 shows the domain used for the dynamical downscaling simulations. In WRF, the planetary boundary layer simulations use the Noah land surface model (Tewari et al. 2004), the Yonsei-University boundary layer scheme (Hong et al. 2006), and the Monin-Obukhov surface layer scheme (Monin and Obukhov 1954). The microphysics parameterizations use the WRF Single-Moment five-class schemes (Hong et al. 2004). The CAM3 (version 3 of NCAR Community Atmosphere Model) radiation scheme

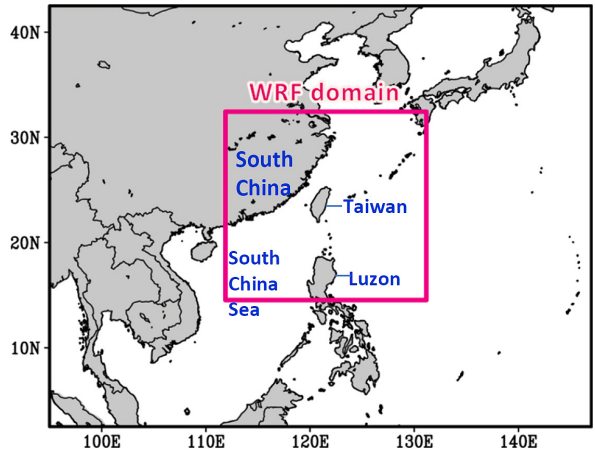


Fig. 1. Geographic location of Taiwan and model domain (dark pink box) used in WRF simulations. The land areas are shaded in gray.

(Collins et al. 2004) is used and the RCP8.5 greenhouse gas (GHG) concentration is considered in the longwave radiation calculation. No cumulus parameterizations are applied for reasons given in Huang et al. (2016c). Spectral nudging (Miguez-Macho et al. 2004) is applied to the atmospheric conditions only and not to the boundary layer. The wavenumber used for the spectral nudging in WRF is 4, the cutoff wavelength is approximately $2000 \text{ km}/4 = 500 \text{ km}$, and the meso-alpha scale feature of global models is kept. The nudged variables are horizontal winds, temperature, and geopotential height from top of the planetary boundary layer to the top of the model. The nudging coefficient is 0.0003 s^{-1} , which is the default value in WRF. These WRF settings follow Huang et al. (2016a, b, c). The sea surface temperature (SST) warming pattern used in HiRAM, MRI global model runs, and HiRAM-WRF, MRI-WRF regional runs are the same, which is the multi-model ensemble mean of future changes (between 2075–2099 and 1979–2003) in long-term climatological means and linear trends projected by 28 CMIP5 models. This SST warming pattern is the same as the ensemble mean pattern used in Kitoh and Endo (2016) and Kusunoki (2018). In this study, only this SST warming pattern is added to the observed monthly SST that retained the observed interannual variability in 1979–2003. The four SST warming patterns defined by Mizuta et al. (2014) based on cluster analysis were not used in this study.

2.2 Observational data and methodology

To evaluate the capabilities of the models in illus-

trating the characteristics of extreme precipitation in Taiwan, we adopted the remapping daily gridded local precipitation data during May and June of 1979–2003 as the observational reference. The gridded precipitation data were provided by the Taiwan Climate Change Projections and Information Platform (TCCIP; <http://tccip.ncdr.nat.gov.tw/v2/index.aspx>), with a horizontal resolution of 5 km. The climatological mean of Mei-Yu season precipitation (denoted as P_{av} ; unit: mm day^{-1}) at the present-day (future) were obtained by averaging the precipitation on all days of May and June from 1979–2003 (2075–2099).

To quantitatively clarify the changes in extreme precipitation events, many studies (e.g., Haylock et al. 2006; Nowbuth 2010; Bürger et al. 2012; Ning et al. 2015; Kim et al. 2018) have adopted the Statistical and Regional dynamical Downscaling of Extremes (STARDEX; https://crudata.uea.ac.uk/projects/stardex/deis/Core_Indices.pdf) indices suggested by the European Union. In this study, two frequently used core indices, prec90p and R90N , from STARDEX were adopted to help quantitatively measure the extreme precipitation activities (including intensity and frequency). The prec90p (unit: mm day^{-1}), which represents the 90th percentile of rainfall intensity, is

obtained by the following steps. First, all examined rainy days (defined as days with precipitation $> 0.1 \text{ mm day}^{-1}$) are ranked from small to large based on the magnitude of their related daily precipitation area-averaged over Taiwan. Second, the value of the area-averaged precipitation intensity ranked at the 90th percentile (i.e., top 10 %) is defined as prec90p . Then, days with the daily precipitation area-averaged over Taiwan larger than prec90p were selected to make the composites of intensity for extreme precipitation events (denoted as PR90).

Table 1 reports the present-day values of prec90p estimated from the observations and models. It should be noted that a model with a more realistic prec90p value (i.e., the value for a precipitation event ranked at the 90th percentile) would not necessarily imply a more realistic PR90 (i.e., the average value for cases with precipitation ranked above the 90th percentile) (e.g., Acharya et al. 2017). The R90N (unit: days per MJ), which represents the number of days with daily precipitation intensity larger than prec90p , was counted for each grid over the domain of Taiwan (Fig. 2a) to make the composites of occurrence frequency for extreme precipitation events. In this study, the thresholds used for the composites of selected variables

Table 1. The value of daily precipitation (unit: mm day^{-1}) area-averaged over Taiwan ranked at the 90th percentile of the data during May and June of 1979–2003 (denoted as prec90p).

	Observation	HiRAM	MRI	HiRAM-WRF	MRI-WRF
prec90p	28.9	27.23	22.35	26.49	21.18

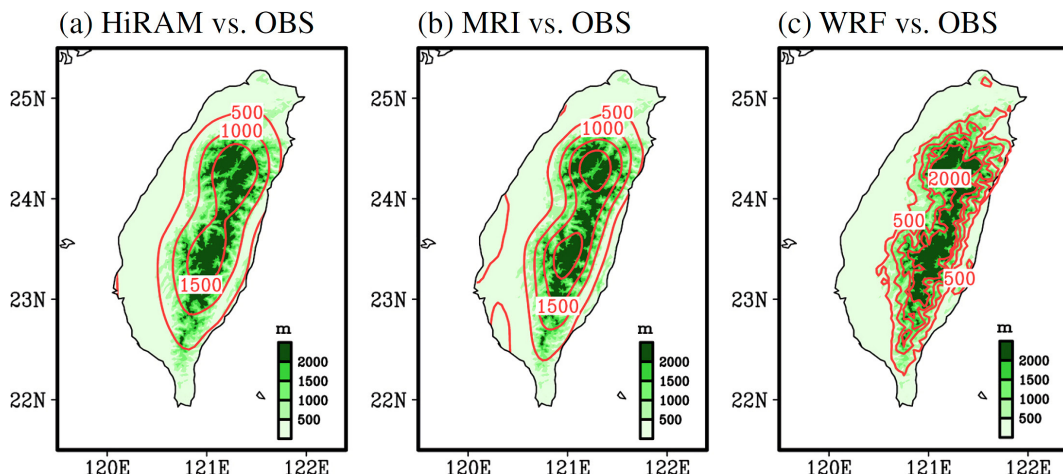


Fig. 2. Topography of Taiwan obtained from the observation (shaded) and models (contours) of (a) HiRAM, (b) MRI, and (c) WRF. The color scale is given in the bottom right. The contour interval is 500 meters.

(PR90 and R90N) in the future are the same as those used for the composites in the present-day.

In Section 4, the percentage of projected changes of selected variables relative to the present-day values is obtained based on Eq. (1):

$$\text{Percentage (\%)} = \frac{\text{future} - \text{present}}{\text{present}} \times 100\%. \quad (1)$$

To determine the significance of projected changes (i.e., future minus present) in selected variables, a two-tailed student's *t*-test was used based on the effective degrees of freedom (Von Storch and Zwiers 1999).

3. Present-day simulation

From the observational topography (shaded area in Fig. 2), it is noted that Taiwan is characterized by a complex local topography, with north-south-oriented high mountains located at the central region. Divided by the central high mountains, the slope in the east of Taiwan is steeper than that in the west where vast plains are located. The comparison of these observational characteristics with the topography used in HiRAM (red contours in Fig. 2a) and MRI (red contours in Fig. 2b) shows that the complicated high mountain range over central Taiwan cannot be represented well in either HiRAM or MRI. In contrast, the topography used in WRF (red contours in Fig. 2c) depicts a more delicate Taiwan terrain structure. Previous studies have suggested that terrain plays an important role in modulating precipitation (e.g., Smith 1980, 1989; Ogura and Yoshizaki 1988; Wang and Chang 2012). Furthermore, according to the review of Kitoh (2017), the improvements in precipitation simulation by regional climate models (as compared to global climate models) might be caused by the better representation of topography and underlying land surface, with an urban canopy scheme included in some regional models. As WRF has a better representation of topography than HiRAM and MRI (Fig. 2), a dynamical downscaling simulation using WRF might produce a more realistic representation of Mei-Yu season precipitation in Taiwan.

To prove the above assumption, we first evaluated the spatial distribution of the climatological mean of Mei-Yu season precipitation (Pav; Fig. 3) over Taiwan extracted from observation and model simulations at the present-day (1979–2003). From the observation (Fig. 3a), it is noted that Pav generally has maximum values over central and southwest Taiwan, where the windward side of the mountains frequently interact

with the prevailing southwesterly monsoonal flow (Wang et al. 2005). For HiRAM (Fig. 3b) and MRI (Fig. 3c), the distribution of maximum values of Pav is mostly located over eastern Taiwan. In contrast, HiRAM-WRF (Fig. 3e) and MRI-WRF (Fig. 3f) simulated the maximum mean precipitation values mainly in the central mountain region of Taiwan. Visually, it seems that HiRAM-WRF and MRI-WRF are more capable than HiRAM and MRI in depicting the spatial distribution of Pav in Taiwan. To provide the statistical evidence for this suggestion, we evaluated the spatial correlation coefficient (SCC) and the root-mean-square error (RMSE) between the simulated and the observed Pav and summarize the results in Fig. 3d. Indeed, compared to the Pav simulated by HiRAM-WRF and MRI-WRF, the Pav simulated by HiRAM and MRI have higher RMSE values and lower SCC values. However, it should be noted that even though the downscaled simulation of precipitation distribution is more realistic than that of the related global model, it still suffers some eastward displacement. This bias represents the fact that HiRAM-WRF and MRI-WRF tend to produce more precipitation in the high mountains than on the windward side of the high mountains (i.e., the areas with larger Pav in the observation). As inferred from this result, it is expected that a similar bias might also exist in the dynamical downscaling simulation of extreme precipitation over Taiwan.

To clarify the above inference, we evaluated the model performances in simulating the composites of precipitation intensity for extreme events (i.e., PR90; see Section 2 for definition) at the present-day. From the observation (Fig. 4a), it is noted that the maximum values of PR90 are located in the central and southwest region of Taiwan, which is similar to that of Pav (Fig. 3a). The close relationship between Pav and PR90 over Taiwan is revealed not only during the Mei-Yu season but also in other seasons as well (not shown). However, when examining the larger domain of variables shown in Fig. 3a and Fig. 4a (not shown), we found that the similarity between Pav and PR90 does not appear over other nearby land areas (e.g., Southeast China). This suggests that the aforementioned close relationship between Fig. 3a and Fig. 4a is a local feature (i.e., location dependent).

Focusing on the domain of Taiwan, the similarity between Pav and PR90 is revealed not only in the observation but also in the model simulations. For example, the aforementioned model bias regarding the pattern shift of Pav is also revealed in the simulation of PR90 in both HiRAM (Fig. 4b) and MRI (Fig. 4c) simulations. Compared to Figs. 4b and 4c, the related

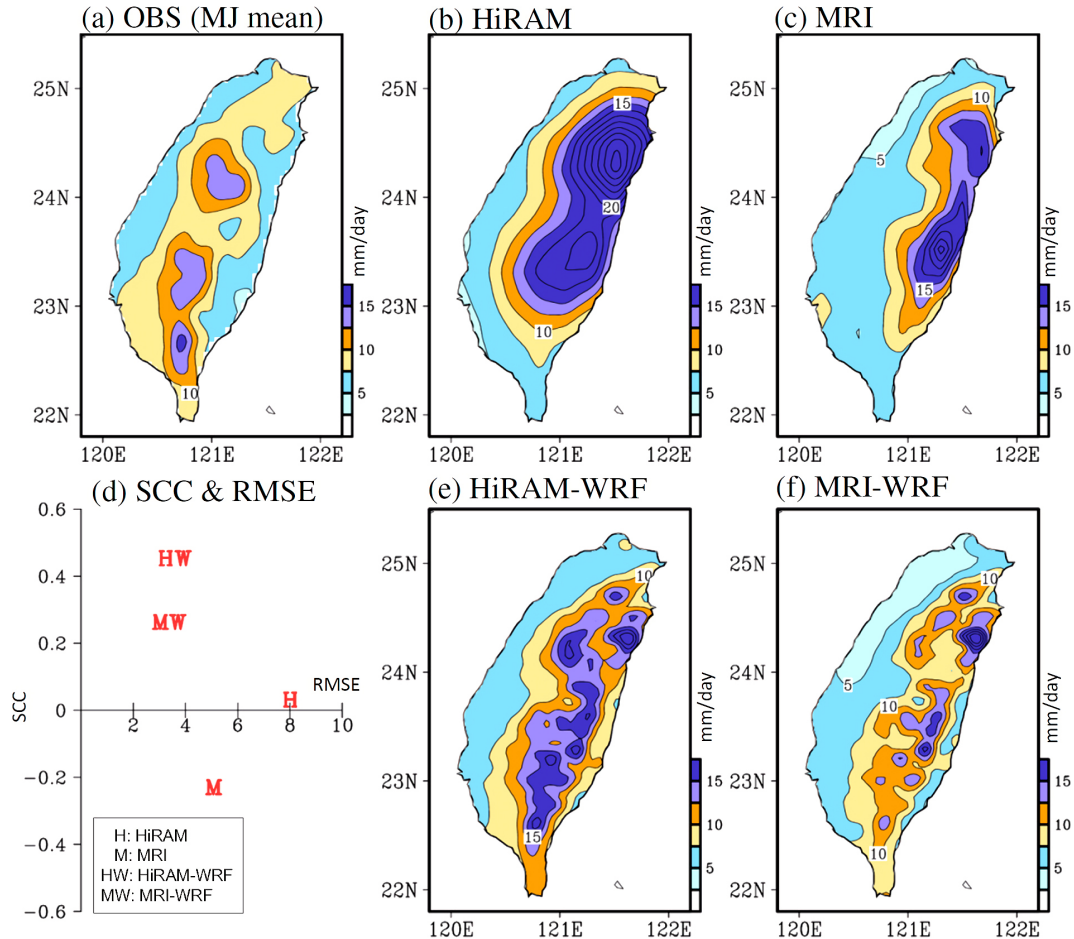


Fig. 3. The spatial distribution of mean precipitation (denoted as Pav, unit: mm day^{-1}) over Taiwan extracted from (a) the observation and the model simulations of (b) HiRAM, (c) MRI, (e) HiRAM-WRF, and (f) MRI-WRF, averaged during May and June of 1979–2003. The spatial correlation coefficient (SCC) and the root-mean-square error (RMSE; unit: mm day^{-1}) obtained from the comparison between (a) and (b, c, e, and f) are documented in (d).

dynamical downscaling simulations (Figs. 4e, f) are more capable of representing the location of maximum PR90 over the central mountain range that are similar to the observations. Statistical examinations of the SCC and RMSE for the comparison between observed and simulated PR90 (see Fig. 4d) show that the dynamical downscaling simulations (i.e., HiRAM-WRF and MRI-WRF) have a better skill (i.e., higher SCC value and lower RMSE value) than its related global models (i.e., HiRAM and MRI) in depicting the spatial distribution of PR90. However, similar to what was inferred from the result of Fig. 3, HiRAM-WRF and MRI-WRF also suffer some eastward displacement in the simulation of PR90, even though the bias is much smaller compared to what is revealed in HiRAM and

MRI.

In Fig. 4, the difference between HiRAM-WRF and MRI-WRF is clearly observed. Kitoh (2017) has noted that because the boundary conditions of regional downscaling models originally come from global models, the large-scale circulation component of the projections in the regional downscaling models will not change much from that of the parent global models. Consistent with Kitoh (2017), we note that the large difference between HiRAM-WRF and MRI-WRF in Fig. 4 comes from the large difference between their parent global models (i.e., HiRAM and MRI). On the other hand, despite the fact that the simulated magnitudes of Pav and PR90 over Taiwan by HiRAM-WRF and MRI-WRF are smaller than those simulated by

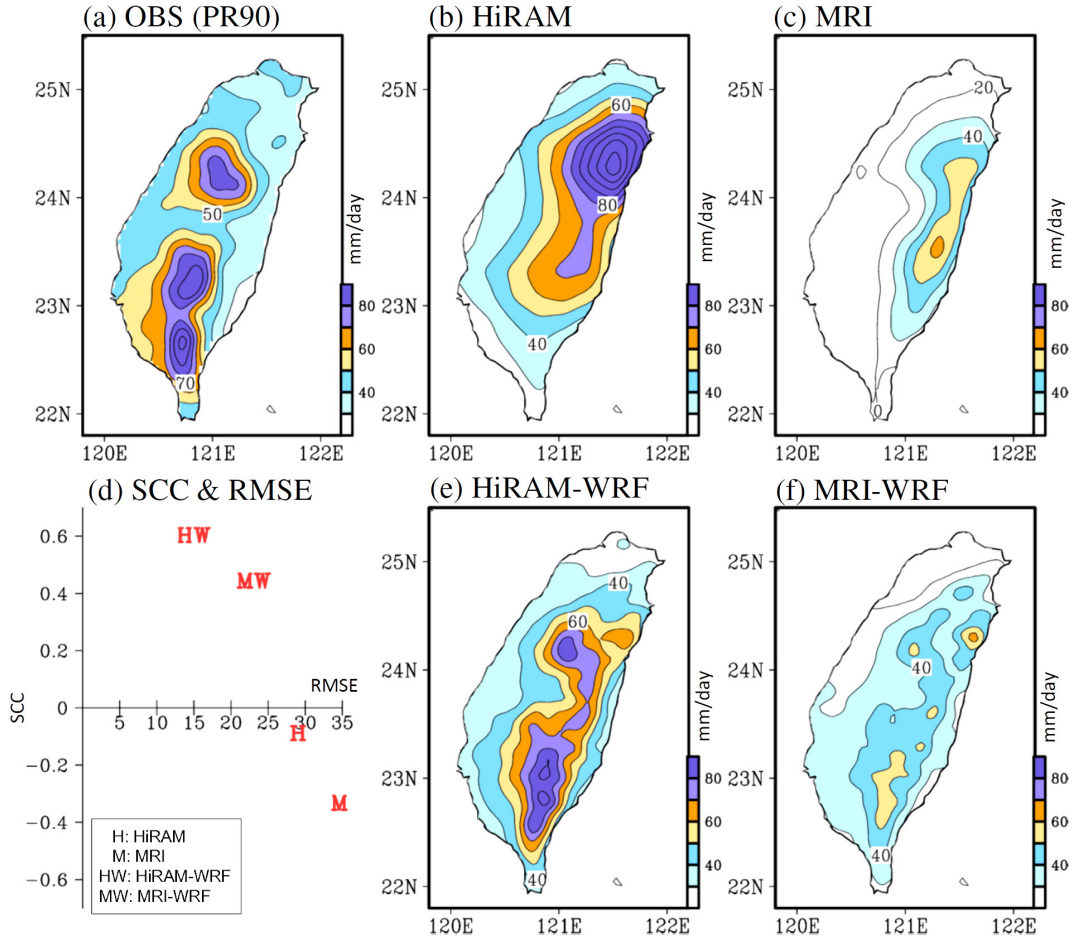


Fig. 4. As in Fig. 3, but for the spatial distribution of composites of extreme precipitation intensity, i.e., PR90 (see Section 2 for definition), estimated by (a) the observation and (b, c, e, and f) the models. The spatial correlation coefficient (SCC) and the root-mean square error (RMSE; unit: mm day^{-1}) obtained from the comparison between (a) and (b, c, e, and f) are documented in (d).

their respective global models, the SCC and RMSE of HiRAM-WRF and MRI-WRF are closer to observations than the global models (Fig. 4d). This suggests that the dynamical downscaling method adds value to the simulation of Pav and PR90.

Next, we compared the observed and simulated spatial distributions of R90N (see Section 2 for definition) at the present-day to determine the abilities of the models to illustrate the occurrence frequency of extreme precipitation. It is noted that the areas with larger R90N values (Fig. 5) are also the areas with larger PR90 values (Fig. 4). This feature is true for both the observation and the model simulations. Relative to their related global models, HiRAM-WRF and MRI-WRF have higher SCC values and lower RMSE

values in simulating R90N over Taiwan (see Fig. 5d). The consistent findings revealed in Figs. 3–5 lead to a suggestion that the dynamical downscaling approach not only add values in the simulation of mean status of precipitation but also add values in the simulation of extreme precipitation activities (including intensity and frequency) during the Mei-Yu seasons. Based on these results, we then adopted only HiRAM-WRF and MRI-WRF for the rest of the examinations and discussions of issues related to future projections.

4. Future projection

Figure 6 shows the percentage of projected changes (see Eq. 1 for method of calculation) in Pav, PR90, and R90N area-averaged over Taiwan, estimated by

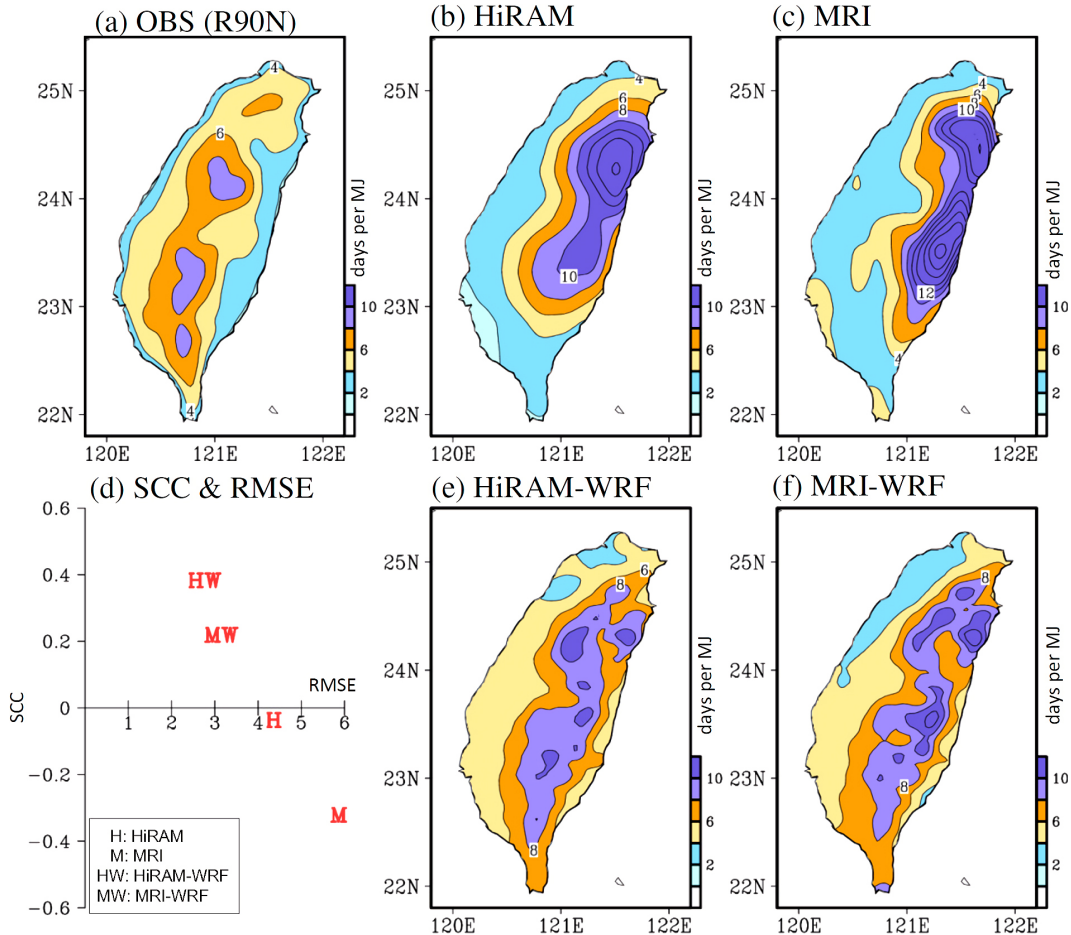


Fig. 5. Similar to Fig. 4, but for the spatial distribution of composites of extreme precipitation frequency, i.e., R90N (see Section 2 for definition), estimated by (a) the observation and (b, c, e, and f) the models. The spatial correlation coefficient (SCC) and the root-mean square error (RMSE; unit: days per MJ) obtained from the comparison between (a) and (b, c, e, and f) are documented in (d).

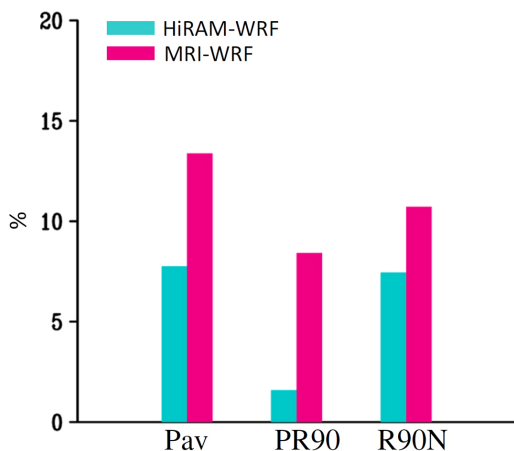


Fig. 6. The percentage (%) of projected changes (future minus present) of selected variables (Pav, PR90, and R90N) area-averaged over all of Taiwan, relative to the corresponding area-averaged values at the present-time, i.e., $\{[(\text{future} - \text{present}) / \text{present}] \times 100\%\}$, estimated by HiRAM-WRF and MRI-WRF. None of the values pass the 90 % significance *t*-test. The Student's *t*-test of Pav is calculated with the annual mean value from each year, following Kimoto et al. (2005).

HiRAM-WRF and MRI-WRF during the Mei-Yu seasons of the future (2075–2099) and the present (1979–2003). Overall, both HiRAM-WRF and MRI-WRF project an increase (< 15 %) in Pav, PR90, and R90N area-averaged over Taiwan in the future compared to the present. Despite the magnitude difference between HiRAM-WRF and MRI-WRF, the sign of projected changes shown in Fig. 6 is found not to be model dependent. However, statistical examinations show that none of the changes in Fig. 6 passed the significance test with 90 % confidence intervals. This leads us to question whether the local community should worry about the future changes in Mei-Yu season extreme precipitation changes in Taiwan. This issue is examined further herein.

In view of earlier literature (e.g., Huang and Wang 2017), most studies that examined the projected

changes in Mei-Yu season precipitation over Taiwan have mainly considered Taiwan as a whole but have not paid attention to regional differences. This study is different from previous studies, as it is also interested in understanding (1) whether or not there is a regional difference in the projected changes in Mei-Yu season extreme precipitation in Taiwan and (2) how the agricultural regions over Taiwan will likely be affected by the Mei-Yu season extreme precipitation changes in the future. To answer the first question, we examined the spatial distribution of the projected changes in Pav, PR90, and R90N over Taiwan estimated by HiRAM-WRF and MRI-WRF, based on the differences between the Mei-Yu seasons of the future (2075–2099) and the present (1979–2003). The results are given in Fig. 7. Notably, the distribution of the projected changes in Pav, PR90, and R90N (see Fig. 7)

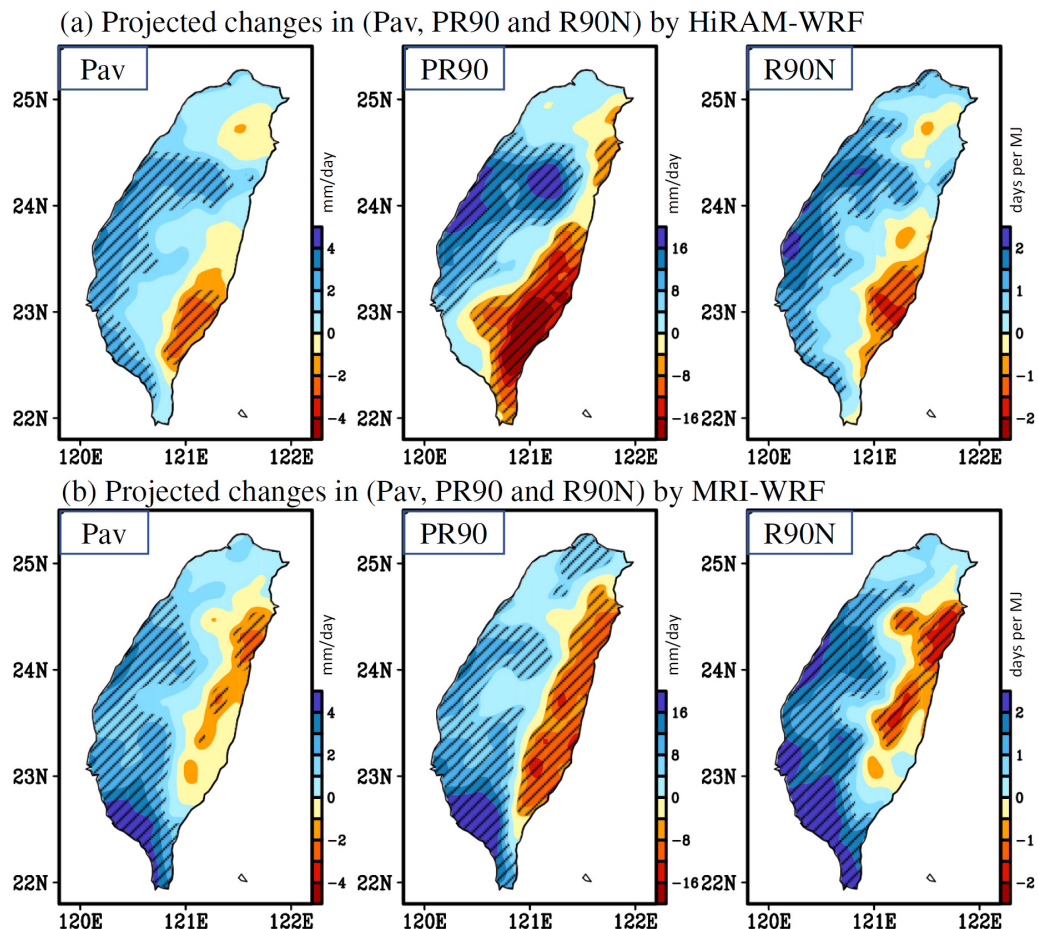


Fig. 7. Projected changes (i.e., future minus present) of selected variables (Pav, PR90, and R90N) estimated by (a) HiRAM-WRF and (b) MRI-WRF. The areas with significant changes at the 90 % confidence interval over Taiwan are marked by a slash.

is characterized by a clear east-west contrast, with positive (negative) values in the west (east) side of the mountain range. Such a similarity between the projected changes in Pav, PR90, and R90N leads to the suggestion that not only the mean precipitation but also the extreme precipitation will enhance (suppress) in western (eastern) Taiwan in the future during the Mei-Yu seasons. Most importantly, unlike the area-averaged values over the whole Taiwan region (Fig. 6) that do not reveal significant changes due to the cancellation between positive (western side) and negative (eastern side) changes, the changes in Pav, PR90, and R90N become significant when examining their regional distributions (Fig. 7).

Furthermore, based on the geographical location and the sign of projected changes shown in Fig. 7, we divided the agricultural regions of Taiwan into three areas (Fig. 8) to examine the related future changes. Figure 9 shows the percentage change in the projected differences between the future and the present (see Eq. 1 for method of calculation) for the selected indices (i.e., Pav, PR90, and R90N) area-averaged over the northwestern agricultural region (blue slash in Fig. 8), the southwestern agricultural region (red dot in Fig. 8), the eastern agricultural region (purple backslash in Fig. 8), and all of the agricultural regions of Taiwan.

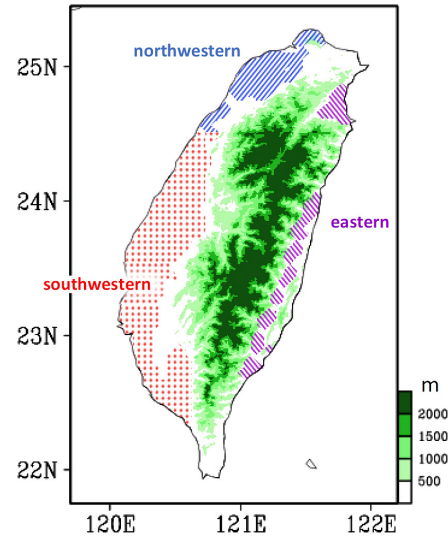


Fig. 8. The topography (shaded) and agricultural region (marked areas) of Taiwan. Based on features revealed in Fig. 7, the agricultural regions are divided into three, including northwestern (blue slash), southwestern (red dot), and eastern (purple backslash) agricultural regions of Taiwan. The information for agricultural regions are provided by the Council of Agriculture, Executive Yuan in Taiwan (<http://aldoc.coa.gov.tw/aldoc/>).

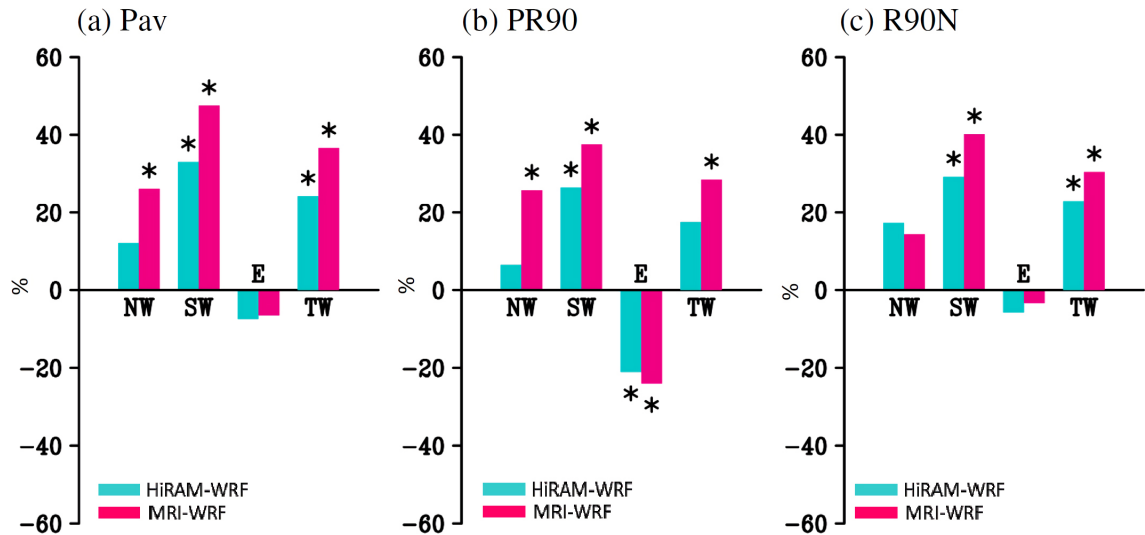


Fig. 9. Similar to Fig. 6, but for the percentage (%) of projected changes (future minus present) of selected variables, (a) Pav, (b) PR90, and (c) R90N, area-averaged over selected agricultural regions, estimated by HiRAM-WRF and MRI-WRF based on Eq. (1) listed in Section 2. The abbreviations of NW, SW, E, and TW represent the agricultural regions (marked areas in Fig. 8) of northwestern Taiwan, southwestern Taiwan, eastern Taiwan, and Taiwan as a whole, respectively. The change in percentage significant at 90 % confidence intervals is marked by an asterisk. The Student's *t*-test of Pav is calculated with the annual mean value from each year, following Kimoto et al. (2005).

For the northwestern agricultural region, projected increases in Pav, PR90, and R90N are revealed in both the HiRAM-WRF and MRI-WRF simulations, but only the increase in Pav and PR90 projected by MRI-WRF passed the significance test. In contrast, the southwestern agricultural region shows a significant increase (more than 25%; see Fig. 9) in Pav, PR90, and R90N, as projected by HiRAM-WRF and MRI-WRF. For the eastern agricultural region, decreases in Pav, PR90, and R90N are projected by both HiRAM-WRF and MRI-WRF; however, only the projected changes in PR90 passed the significance test. Most of Pav, PR90, and R90N (except PR90 in HiRAM-WRF) are projected to significantly increase in the future, when considering the agricultural regions of Taiwan as a whole.

Obviously, when looking into the regional differences over the agricultural regions, the potential impact of future changes in the Mei-Yu season extreme precipitation in Taiwan becomes nonignorable. These findings highlight the importance of examining the regional differences over complex terrain (such as Taiwan), in addition to the frequently discussed area-averaged values, when projecting the future changes of extreme precipitation activities. This information is particularly important to the local community, because it suggests that different long-term plans are necessary for different regions to prevent the potential damage from future changes in extreme precipitation during the Mei-Yu seasons.

Notably, because the main difference between Figs. 6 and 9 is the mountainous region being included or not, one might infer from Figs. 6 and 9 that the projected changes in Pav, PR90, and R90N for the mountainous region are not significant. Indeed, by

calculating the changes over the mountainous region for Pav, PR90, and R90N (not shown), we note that the changes are small (due to the cancellation between the positive values in most western mountainous areas and the negative values in most eastern mountainous areas) and not significant (at the 90% confidence interval).

5. Possible explanation of projected change in extreme precipitation activities

What might be the causes for the extreme precipitation to become more (less) frequent and more (less) intense over western (eastern) Taiwan in the future than in the present-day? Previous observational studies have suggested that the formation of Mei-Yu season heavy precipitation events over Taiwan might be attributed to the intensification of (1) orographic lifting (i.e., windward side) of southwesterly monsoon wind (e.g., Smith 1989; Chen et al. 2005; Sampe and Xie 2010) and (2) water vapor flux convergence (e.g., Johnson and Bresch 1991; Huang and Chen 2015). Therefore, examining the changes in these two factors between the future and present-day might give us a clue for determining the projected changes in Mei-Yu season extreme precipitation activities over Taiwan. This is discussed below.

First, prior to detailed examination, we evaluated the capability of models in simulating the present-day atmospheric circulation. Here, the present-day observed wind fields were extracted from Modern Era Retrospective-Analysis for Research and Applications (MERRA) reanalysis data (Rienecker et al. 2011), following Huang et al. (2016c). Figure 10 shows composites of the low-level circulation for the Mei-Yu season extreme precipitation days (i.e., days with

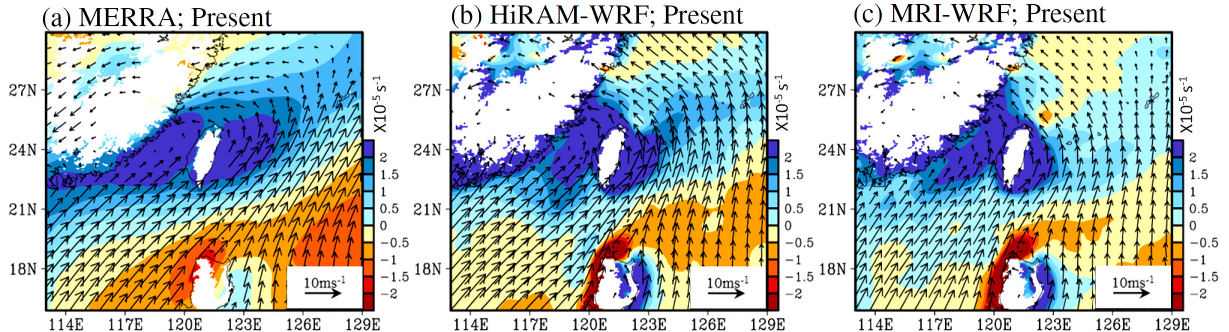


Fig. 10. Composites of low-level circulation superimposed with vorticity at 925 hPa for the extreme rainfall cases ranked above the 90th percentile during the present-day: (a) MERRA (the reanalysis data), (b) the HiRAM-WRF simulation, and (c) the MRI-WRF simulation.

area-averaged daily precipitation ranked in the top 10 %) extracted from present-day MERRA reanalysis data (Fig. 10a), HiRAM-WRF (Fig. 10b) and MRI-WRF (Fig. 10c). By comparing Fig. 10a with Figs. 10b, c, it can be seen that present-day simulations with both HiRAM-WRF and MRI-WRF are capable of reproducing the MERRA reanalysis data that Taiwan is under the influence of southwesterly monsoonal flow at the low level. To quantitatively evaluate the wind fields, we calculated the spatial correlation of vorticity between Fig. 10b (Fig. 10c) and Fig. 10a, and the value is larger than 0.73 (0.68) and is significant at the 90 % confidence interval.

After verifying the capability of the WRF dynamical downscaling method in simulating present-day

atmospheric circulation, we compared the differences between the composites of low-level circulation superimposed with precipitation for the Mei-Yu season extreme precipitation days in the present-day (Figs. 11a, b) and its projected changes in the future (Figs. 11c, d). As seen in Fig. 11, HiRAM-WRF and MRI-WRF both project that the low-level southwesterly monsoonal flow along the coastal regions of South China will be stronger in the future than in the present-day, despite the difference that the projected change in wind direction is more southerly in HiRAM-WRF but more westerly in MRI-WRF. Note that western (eastern) Taiwan is on the windward (leeward) side of the intensification of low-level southwesterly monsoonal winds. Considering the effect of orograph-

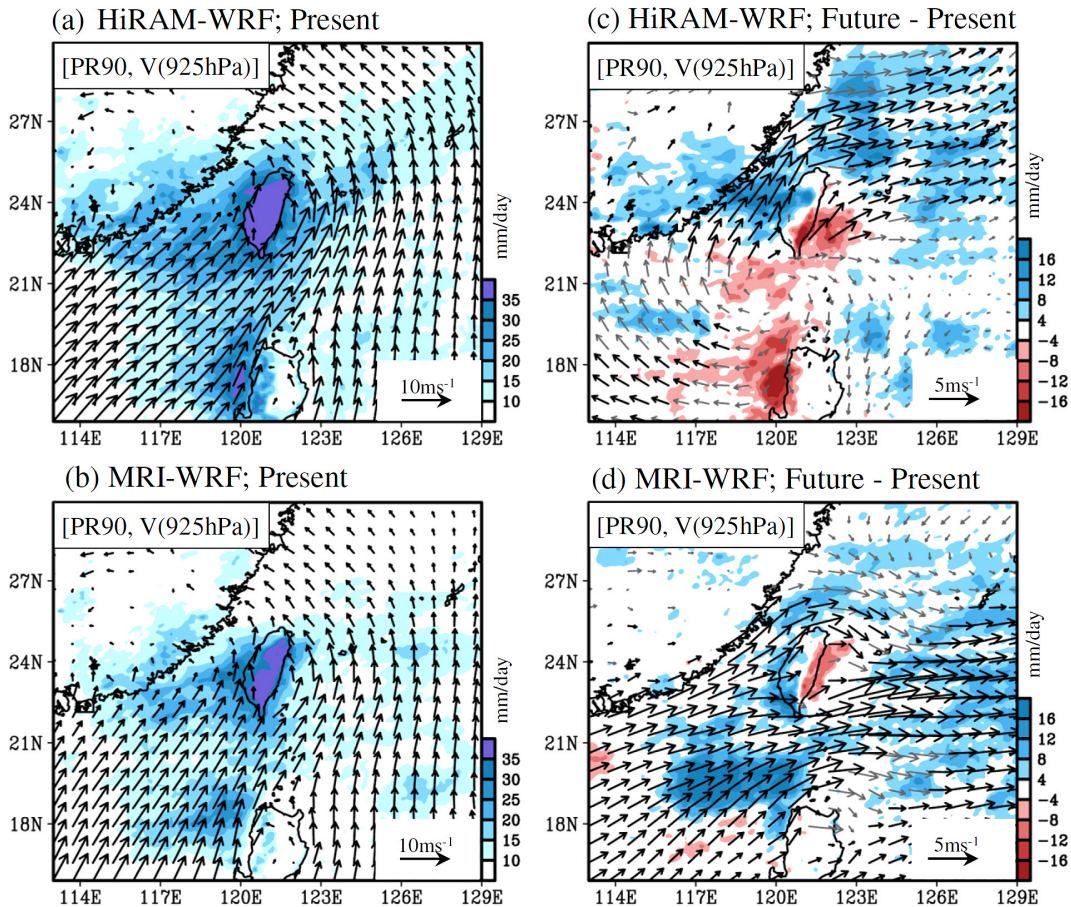


Fig. 11. Composites of precipitation intensity (PR90; shaded) and low-level circulation at 925 hPa [V (925hPa); vectors] for the extreme precipitation events ranked at the top 10 %, estimated by (a) HiRAM-WRF and (b) MRI-WRF present-day simulations. (c) and (d) correspond to (a) and (b) but for the difference between the future (2075–2099) and the present-day (1979–2003) simulations of [PR90, V (925hPa)] of extreme precipitation events. In (c) and (d), the changes in vectors pass (do not pass) the 90 % significance t -test are colored by black (gray), and only the areas with significant precipitation changes (at 90 % confidence intervals) are shaded.

ic lifting, it is reasonable to find that the low-level wind convergence is projected to be enhanced (suppressed) over western (eastern) Taiwan (figure not shown). This change in dynamical lifting and associated low-level wind convergence are the possible causes explaining why HiRAM-WRF and MRI-WRF both project that extreme precipitation will become more (less) frequent over western (eastern) Taiwan.

Many studies examining the characteristics and causes of precipitation changes over Taiwan during the past have suggested that the changes in precipitation over Taiwan are location dependent and occur in response to changes in related atmospheric circulation (e.g., Chen et al. 2010; Chou et al. 2011; Tu and Chou 2013). This suggestion can also explain the projected changes in extreme precipitation over Taiwan and surrounding regions seen in Figs. 11c and 11d that show extreme precipitation will be enhanced (suppressed) over the windward (leeward) side of Taiwan, Southeast China, and Luzon. Notably, according to the definition of PR90, the date of the PR90 composite shown in Fig. 11 is common among all grids. One might question whether the features revealed in Fig. 11 would be drastically changed if different composite dates suitable for only extreme precipitation on the eastern side of Taiwan were selected. To clarify this concern, we conducted additional examinations (not shown) and confirmed that similar features can be found even when composite dates suitable for only the extreme precipitation on the eastern side were selected.

Regarding the causes of past and future changes in atmospheric circulation simulated by various global models, a detailed review of the literatures can be found in Kitoh (2017). Unfortunately, the two global models used in this study (i.e., HiRAM and MRI) do not provide simulations driven by different forcings (e.g., natural variability and anthropogenic forcing). Thus, it is not possible for this study to comment on the main reason driving the past and future changes in circulation shown in Fig. 11. Future studies should be performed to clarify this issue once the data are available for analysis.

Finally, we examined the simulated and projected changes in vertically integrated moisture flux convergence, denoted as $(-\nabla \cdot Q)$, to explain the moisture supply for the extreme precipitation intensity over Taiwan, following Huang et al. (2016c). Here, the calculation of the convergence of vertically integrated moisture flux [denoted as $(-\nabla \cdot Q)$] is based on Eq. (2) as follows:

$$(-\nabla \cdot Q) = -\nabla \cdot \left[\frac{1}{g} \left(\int_{300}^{p_s} Vq \, dp \right) \right], \quad (2)$$

where V denotes the horizontal wind vectors, q is the specific humidity, g is gravity, and p is the pressure level (Chen et al. 1988). As revealed in Figs. 12a and 12b, both HiRAM-WRF and MRI-WRF simulations at the present-day show that the water vapor flux is convergent from nearby regions to Taiwan, and it provides the moisture supply for the formation of extreme precipitation over Taiwan. For the future changes (Figs. 12c, d), HiRAM-WRF and MRI-WRF have both projected more (less) water vapor flux will converge into western (eastern) Taiwan. In association with the water vapor flux changes, extreme precipitation will be more (less) intense over western (eastern) Taiwan.

According to Banacos and Schultz (2005), the moisture flux $(-\nabla \cdot Vq)$ can be separated into $-V \cdot \nabla q$ (advection term) and $-q\nabla \cdot V$ (convergence term), e.g., $-\nabla \cdot Vq = -V \cdot \nabla q - q\nabla \cdot V$. By examining the variables associated with precipitation changes over areas near Taiwan, many studies have shown that $-\nabla \cdot Vq$ is mainly dominated by its related convergence term (e.g., Huang et al. 2015); similar findings are also revealed when we separate Figs. 12c and 12d into related advection and convergence terms (not shown). By examining the projected changes in vertically integrated specific humidity [i.e., $q_{\text{vint}} = \frac{1}{g} \left(\int_{300}^{p_s} q \, dp \right)$], we note that the future change of q_{vint} is positive for all of eastern and western Taiwan (see Figs. 13c, d). In other words, the change in specific humidity (i.e., q) is unlikely to be responsible for the “east-west difference” of sign change in $(-\nabla \cdot V)$. This implies that the east-west difference in $(-\nabla \cdot Q)$ (Figs. 12c, d) is not mainly caused by the spatial changes in moisture (Figs. 13c, d) but rather by the spatial changes in wind circulation (Figs. 11c, d). The projected increase in the low-level moisture amount (Figs. 13c, d) is important in determining the magnitude of $(-\nabla \cdot V)$ as well as the associated magnitude of $(-\nabla \cdot Q)$ (Figs. 12c, d). In other words, the changes in low-level moisture may play an important role in determining whether the changes in moisture flux convergence are significant or not.

In summary, it is suggested that the east-west contrast revealed in the projected changes of occurrence frequency and intensity of Mei-Yu season extreme precipitation over Taiwan are the local responses to the projected changes in large-scale wind circulation and $(-\nabla \cdot Q)$ over the East-Asian monsoon region.

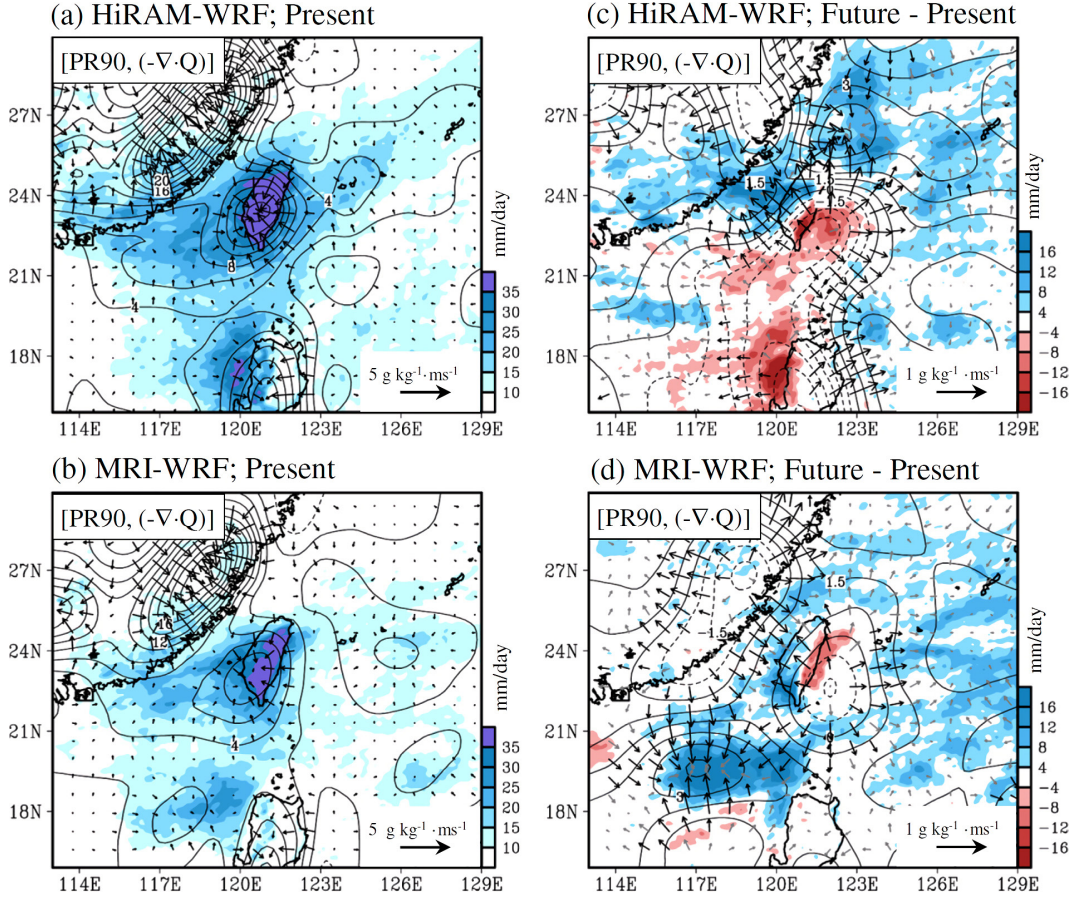


Fig. 12. Composites of convergence of vertically integrated moisture flux [i.e., $(-\nabla \cdot Q)$; contours] superimposed with the related moisture transportation (vectors) and precipitation intensity (PR90; shaded) for the extreme precipitation events ranked at the top 10 %, estimated by (a) HiRAM-WRF and (b) MRI-WRF present-day simulations. (c) and (d) correspond to (a) and (b) but for the difference between the future (2075–2099) and the present-day (1979–2003) simulations of $[PR90, (-\nabla \cdot Q)]$ of extreme precipitation events. In (c) and (d), the changes in vectors pass (do not pass) the 90 % significance t -test are colored by black (gray), and only the areas with significant precipitation changes (at 90 % confidence intervals) are shaded. The dashed contour lines in c and d indicate negative values. The unit of contours is $10^{-5} \text{ kg m}^{-2} \text{s}^{-1}$.

6. Conclusion

This study examines the simulation and future projection of Mei-Yu season extreme precipitation activities over Taiwan based on the dynamical downscaling simulations using WRF driven by HiRAM and MRI (denoted as HiRAM-WRF and MRI-WRF, respectively). From the present-day simulations (1979–2003, historical run), our analyses show that the use of a dynamical downscaling approach (i.e., HiRAM-WRF and MRI-WRF) is more capable than the use of the original global models (i.e., HiRAM and MRI) in simulating the intensity (i.e., PR90) and frequency

(i.e., R90N) of extreme precipitation over Taiwan. In particular, similar to the observations, HiRAM-WRF and MRI-WRF can capture the feature with more intense and more frequent extreme precipitation revealed over the central mountainous areas than the other subregions of Taiwan, while HiRAM and MRI cannot. A possible explanation for the better skill of HiRAM-WRF and MRI-WRF in capturing the extreme precipitation activities in Taiwan is attributed to the fact that the topography used in the dynamical downscaling simulation is closer to the real observed topography.

For the future projections (2075–2099, RCP8.5

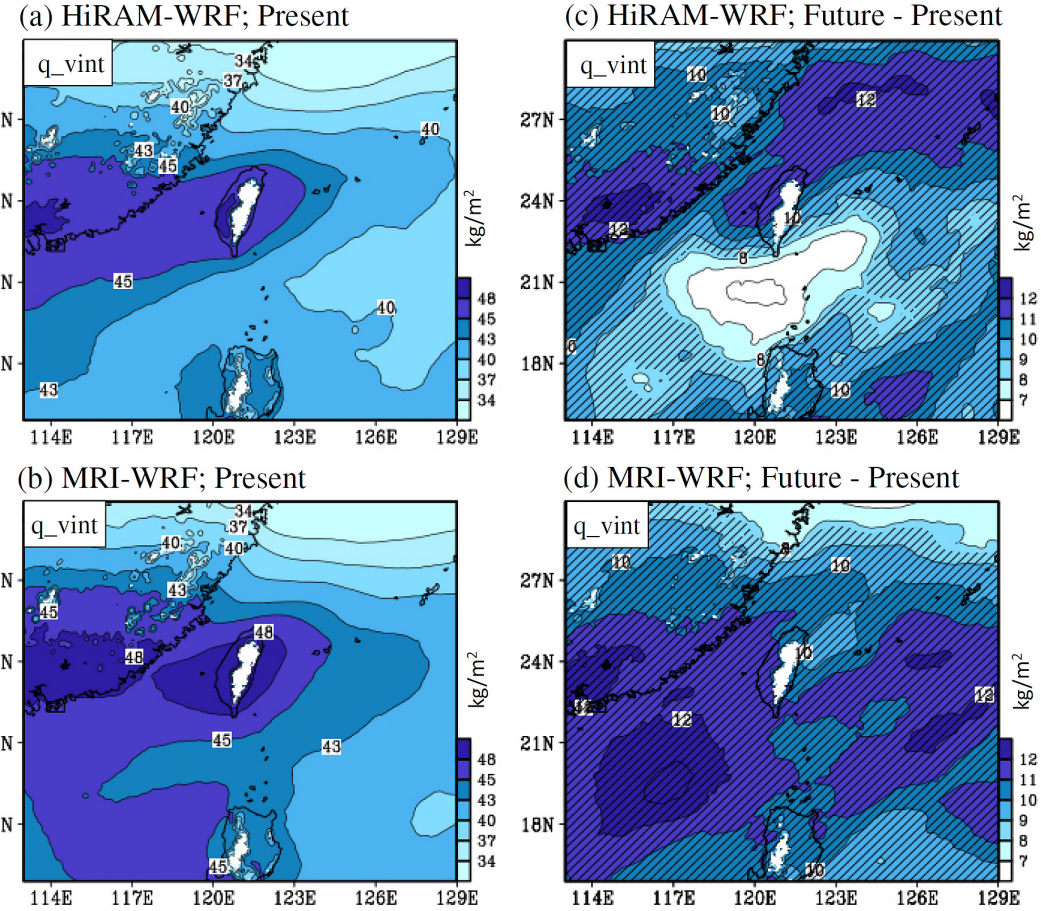


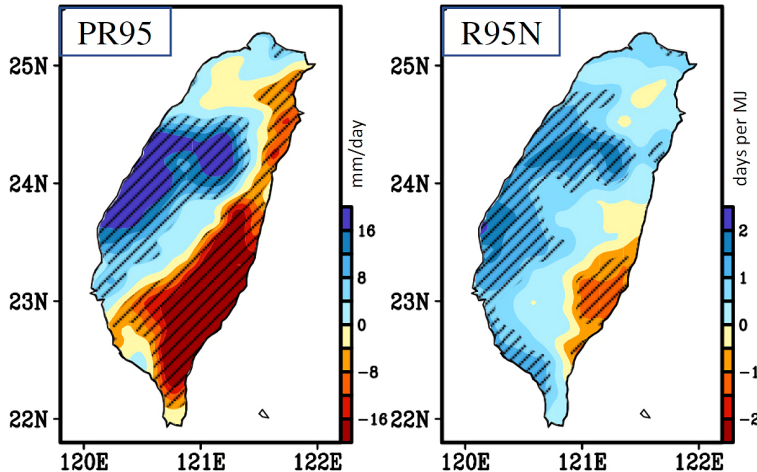
Fig. 13. Composites of vertically integrated specific humidity, denoted as q_{vint} , for the extreme precipitation events ranked at the top 10 %, estimated by (a) HiRAM-WRF and (b) MRI-WRF present-day simulations. (c) and (d) correspond to (a) and (b) but for the difference between the future (2075–2099) and the present-day (1979–2003) simulations of q_{vint} of extreme precipitation events. In (c) and (d), the areas with significant changes (at 90 % confidence intervals) are marked by a slash. The q_{vint} over the mountain areas are not plotted.

scenario), when considering the changes over Taiwan as a whole (i.e., the area-averaged values), HiRAM-WRF and MRI-WRF both project that the Mei-Yu season precipitation will become more frequent and more intense in the future than in the present; however, the projected changes do not pass the significance test. By contrast, when considering the regional differences, HiRAM-WRF and MRI-WRF both project that Mei-Yu season extreme precipitation will increase over western Taiwan but decrease over eastern Taiwan, with most of the areas passing the significance test. The occurrence frequency and intensity of extreme precipitation over the agricultural regions of southwestern Taiwan are projected to significantly increase (more than 25 %) in the future than in the

present. Furthermore, examinations on the related maintenance mechanisms show that the regional difference in the projected changes of extreme precipitation over Taiwan is a local response to the future changes of low-level wind circulation and moisture convergence over the East-Asian monsoon region.

Notably, this is the first study to present the regional difference in the projected changes of Mei-Yu season extreme precipitation with a focus over the agricultural regions of Taiwan. This information is particularly important for the local community when considering long-term plans for different areas in preventing the potential damage caused by the extreme precipitation changes under global warming. In addition to the criterion of the 90th percentile (Fig. 7), we also tested

(a) Projected changes in (PR95 and R95N) by HiRAM-WRF



(b) Projected changes in (PR95 and R95N) by MRI-WRF

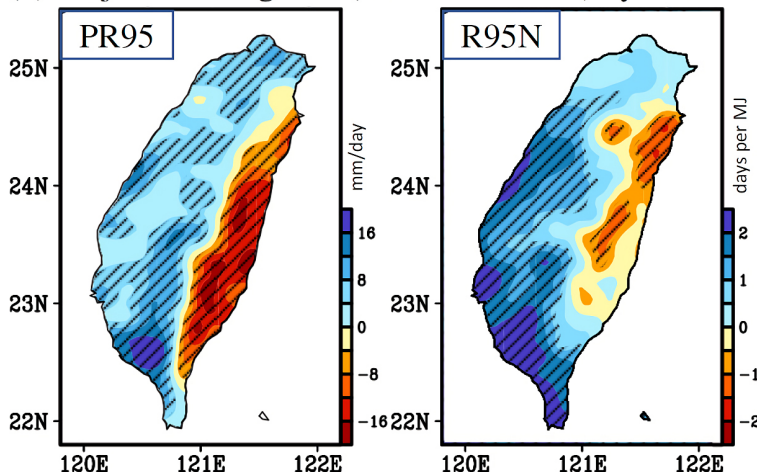


Fig. 14. Similar to Fig. 7, but showing the projected changes (future minus present) in PR95 and R95N estimated by composites of extreme cases ranked above 95th percentile, simulated by (a) HiRAM-WRF and (b) MRI-WRF.

the criterion of the 95th percentile (Fig. 14), and the projected changes are similar between each other, suggesting the findings of this study are robust. However, it should be noted that the projected changes might be different if different emission scenarios are used (e.g., Shiogama et al. 2010; Wang et al. 2017). Additionally, due to the possibility of a difference between the projected changes of large-scale atmospheric circulation between the middle and late 21st century, the projected changes might be different between the middle and late 21st century (e.g., Kim et al. 2018). Further studies are recommended to clarify these issues (different emission scenarios and different simulation periods) in the near future.

Acknowledgments

This work was supported by the Ministry of Science and Technology of Taiwan under MOST 106-2621-M-865-001, MOST 106-2628-M-003-001-MY4, and MOST 107-2625- M-003-002, and by the Integrated Climate Model Advanced Research Program (TOUGOU) of the Ministry of Education, Culture, Sports, Science, and Technology (MEXT) of Japan.

References

- Acharya, N., A. Frei, J. Chen, L. DeCristofaro, and E. M. Owens, 2017: Evaluating stochastic precipitation generators for climate change impact studies of New York City's primary water supply. *J. Hydrometeor.*, **18**, 879–896.
- Agel, L., M. Barlow, J.-H. Qian, F. Colby, E. Douglas, and T. Eichler, 2015: Climatology of daily precipitation and extreme precipitation events in the Northeast United States. *J. Hydrometeor.*, **16**, 2537–2557.
- Banacos, P. C., and D. M. Schultz, 2005: The use of moisture flux convergence in forecasting convective initiation: Historical and operational perspectives. *Wea. Forecasting*, **20**, 351–366.
- Bürger, G., T. Q. Murdock, A. T. Werner, S. R. Sobie, and A. J. Cannon, 2012: Downscaling extremes—An intercomparison of multiple statistical methods for present climate. *J. Climate*, **25**, 4366–4388.
- Chen, C.-S., and Y.-L. Chen, 2003: The rainfall characteristics of Taiwan. *Mon. Wea. Rev.*, **131**, 1323–1341.
- Chen, G. T.-J., C.-C. Wang, and D. T.-W. Lin, 2005: Characteristics of low-level jets over northern Taiwan in mei-yu season and their relationship to heavy rain events. *Mon. Wea. Rev.*, **133**, 20–43.
- Chen, J.-M., J.-L. Chu, C.-F. Shih, and Y.-C. Tung, 2010: Interannual variability of circulation–rainfall relationship in Taiwan during the Mei-yu season. *Int. J. Climatol.*, **30**, 2264–2276.
- Chen, T. C., M. C. Yen, and M. Murakami, 1988: The water vapor transport associated with the 30–50 day oscillation over the Asian monsoon regions during 1979 summer. *Mon. Wea. Rev.*, **116**, 1983–2002.
- Chen, T.-C., S.-Y. Wang, W.-R. Huang, and M.-C. Yen, 2004: Variation of the East Asian summer monsoon rainfall. *J. Climate*, **17**, 744–762.
- Chen, T.-C., W.-R. Huang, and M.-C. Yen, 2011: Interannual variation of the late spring–early summer monsoon rainfall in the northern part of the South China Sea. *J. Climate*, **24**, 4295–4313.
- Chen, Y.-L., Y.-X. Zhang, and N. B.-F. Hui, 1989: Analysis of a surface front during the early summer rainy season over Taiwan. *Mon. Wea. Rev.*, **117**, 909–931.
- Chou, M.-D., C.-H. Wu, and W.-S. Kau, 2011: Large-scale control of summer precipitation in Taiwan. *J. Climate*, **24**, 5081–5093.
- Collins, W. D., P. J. Rasch, B. A. Boville, J. J. Hack, J. R. Mccaa, D. L. Williamson, J. T. Kifhi, B. Briegleb, C. Bits, S. J. Lin, M. Zhang, and Y. Dai, 2004: *Description of the NCAR Community Atmosphere Model (CAM 3.0)*. NCAR Technical Note, NCAR/TN-464+STR, 214 pp. [Available at <https://opensky.ucar.edu/islandora/object/technotes%3A477>.]
- Dulière, V., Y. Zhang, and E. P. Salathé, Jr., 2011: Extreme precipitation and temperature over the U.S. Pacific Northwest: A comparison between observations, reanalysis data, and regional models. *J. Climate*, **24**, 1950–1964.
- Endo, N., J. Matsumoto, and T. Lwin, 2009: Trends in precipitation extremes over Southeast Asia. *SOLA*, **5**, 168–171.
- Haylock, M. R., G. C. Cawley, C. Harpham, R. L. Wilby, and C. M. Goodess, 2006: Downscaling heavy precipitation over the United Kingdom: A comparison of dynamical and statistical methods and their future scenarios. *Int. J. Climatol.*, **26**, 1397–1415.
- Herman, G. R., and R. S. Schumacher, 2016: Extreme precipitation in models: An evaluation. *Wea. Forecasting*, **31**, 1853–1879.
- Hong, S.-Y., J. Dudhia, and S.-H. Chen, 2004: A revised approach to ice microphysical processes for the bulk parameterization of clouds and precipitation. *Mon. Wea. Rev.*, **132**, 103–120.
- Hong, S. Y., Y. Noh, and J. Dudhia, 2006: A new vertical diffusion package with an explicit treatment of entrainment processes. *Mon. Wea. Rev.*, **134**, 2318–2341.
- Huang, W.-R., and K.-C. Chen, 2015: Trends in pre-summer frontal and diurnal rainfall activities during 1982–2012 over Taiwan and Southeast China: Characteristics and possible causes. *Int. J. Climatol.*, **35**, 2608–2619.
- Huang, W.-R., and S.-Y. S. Wang, 2017: Future changes in propagating and non-propagating diurnal rainfall over East Asia. *Climate Dyn.*, **49**, 375–389.
- Huang, W.-R., Y.-H. Chang, C.-T. Cheng, H.-H. Hsu, C.-Y. Tu, and A. Kitoh, 2016a: Summer convective afternoon rainfall simulation and projection using WRF driven by global climate model. Part I: Over Taiwan. *Terr. Atmos. Oceanic Sci.*, **27**, 659–671.
- Huang, W.-R., Y.-H. Chang, H.-H. Hsu, C.-T. Cheng, and C.-Y. Tu, 2016b: Summer convective afternoon rainfall simulation and projection using WRF driven by global climate model. Part II: Over South China and Luzon. *Terr. Atmos. Oceanic Sci.*, **27**, 673–685.
- Huang, W.-R., Y.-H. Chang, H.-H. Hsu, C.-T. Cheng, and C.-Y. Tu, 2016c: Dynamical downscaling simulation and future projection of summer rainfall in Taiwan: Contributions from different types of rain events. *J. Geophys. Res.*, **121**, 13973–13988.
- IPCC, 2013: *Climate Change 2013: The Physical Science Basis. Contribution of Working Group I to the Fifth Assessment Report of the Intergovernmental Panel on Climate Change*. Stocker, T. F., D. Qin, G.-K. Plattner, M. Tignor, S. K. Allen, J. Boschung, A. Nauels, Y. Xia, V. Bex, and P. M. Midgley (eds.), Cambridge University Press, 1535 pp.
- Johnson, R. H., and J. F. Bresch, 1991: Diagnosed characteristics of precipitation systems over Taiwan during the May–June 1987 TAMEX. *Mon. Wea. Rev.*, **119**, 2540–2557.
- Kim, G., D.-H. Cha, C. Park, G. Lee, C.-S. Jin, D.-K. Lee, M.-S. Suh, J.-B. Ahn, S.-K. Min, S.-Y. Hong, and H.-S. Kang, 2018: Future changes in extreme precipitation

- indices over Korea. *Int. J. Climatol.*, **38**, e862–e874.
- Kimoto, M., N. Yasutomi, C. Yokoyama, and S. Emori, 2005: Projected changes in precipitation characteristics around Japan under the global warming. *SOLA*, **1**, 85–88.
- Kitoh, A., 2017: The Asian monsoon and its future change in climate models: A review. *J. Meteor. Soc. Japan*, **95**, 7–33.
- Kitoh, A., and H. Endo, 2016: Changes in precipitation extremes projected by a 20-km mesh global atmospheric model. *Wea. Climate Extremes*, **11**, 41–52.
- Kusunoki, S., 2018: Future changes in precipitation over East Asia projected by the global atmospheric model MRI-AGCM3.2. *Climate Dyn.*, **51**, 4601–4617.
- Loriaux, J. M., G. Lenderink, and A. P. Siebesma, 2017: Large-scale controls on extreme precipitation. *J. Climate*, **30**, 955–968.
- Miguez-Macho, G., G. L. Stenchikov, and A. Robock, 2004: Spectral nudging to eliminate the effects of domain position and geometry in regional climate model simulations. *J. Geophys. Res.*, **109**, D13104, doi:10.1029/2003JD004495.
- Mizuta, R., O. Arakawa, T. Ose, S. Kusunoki, H. Endo, and A. Kitoh, 2014: Classification of CMIP5 future climate responses by the tropical sea surface temperature changes. *SOLA*, **10**, 167–171.
- Mizuta, R., H. Yoshimura, H. Murakami, M. Matsueda, H. Endo, T. Ose, K. Kamiguchi, M. Hosaka, M. Sugi, S. Yukimoto, S. Kusunoki, and A. Kitoh, 2012: Climate simulations using MRI-AGCM3.2 with 20-km grid. *J. Meteor. Soc. Japan*, **90A**, 233–258.
- Monin, A. S., and A. M. Obukhov, 1954: Basic laws of turbulent mixing in the surface layer of the atmosphere. *Tr. Akad. Nauk SSSR Geophys. Inst.*, **24**, 163–187.
- Ning, L., E. E. Riddle, and R. S. Bradley, 2015: Projected changes in climate extremes over the northeastern United States. *J. Climate*, **28**, 3289–3310.
- Nowbuth, M. D., 2010: Assessing climate variability using extreme rainfall and temperature indices. *Univ. Mauritius Res. J.*, **16**, 196–206.
- Ogura, Y., and M. Yoshizaki, 1988: Numerical Study of orographic-convective precipitation over the eastern Arabian Sea and the Ghat Mountains during the summer monsoon. *J. Atmos. Sci.*, **45**, 2097–2122.
- Park, C., S.-K. Min, D. Lee, D.-H. Cha, M.-S. Suh, H.-S. Kang, S.-Y. Hong, D.-K. Lee, H.-J. Baek, K.-O. Boo, and W.-T. Kwon, 2016: Evaluation of multiple regional climate models for summer climate extremes over East Asia. *Climate Dyn.*, **46**, 2469–2486.
- Rienecker, M. M., M. J. Suarez, R. Gelaro, R. Todling, J. Bacmeister, E. Liu, M. G. Bosilovich, S. D. Schubert, L. Takacs, G.-K. Kim, S. Bloom, J. Chen, D. Collins, A. Conaty, A. da Silva, W. Gu, J. Joiner, R. D. Koster, R. Lucchesi, A. Molod, T. Owens, S. Pawson, P. Pegion, C. R. Redder, R. Reichle, F. R. Robertson, A. G. Ruddick, M. Sienkiewicz, and J. Woollen, 2011: MERRA: NASA's Modern-Era Retrospective Analysis for Research and Applications. *J. Climate*, **24**, 3624–3648.
- Sampe, T., and S.-P. Xie, 2010: Large-scale dynamics of the meiyu-Baiu rainband: Environmental forcing by the westerly jet. *J. Climate*, **23**, 113–134.
- Shi, X., and D. R. Durran, 2015: Estimating the response of extreme precipitation over midlatitude mountains to global warming. *J. Climate*, **28**, 4246–4262.
- Shiogama, H., S. Emori, K. Takahashi, T. Nagashima, T. Ogura, T. Nozawa, and T. Takemura, 2010: Emission scenario dependency of precipitation on global warming in the MIROC3.2 model. *J. Climate*, **23**, 2404–2417.
- Skamarock, W. C., J. B. Klemp, J. Dudhia, D. O. Gill, D. M. Barker, M. G. Duda, X. Y. Huang, W. Wang, and J. G. Powers, 2008: *A description of the Advanced Research WRF version 3*. NCAR Technical Note NCAR/TN-475+STR. [Available at <http://opensky.ucar.edu/islandora/object/technotes:500>.]
- Smith, R. B., 1980: Linear theory of stratified hydrostatic flow past an isolated mountain. *Tellus*, **32**, 348–364.
- Smith, R. B., 1989: Mountain-induced stagnation points in hydrostatic flow. *Tellus A*, **41**, 270–274.
- Suzuki, K., G. Stephens, A. Bodas-Salcedo, M. Wang, J.-C. Golaz, T. Yokohata, and T. Koshiro, 2015: Evaluation of the warm rain formation process in global models with satellite observations. *J. Atmos. Sci.*, **72**, 3996–4014.
- Tewari, M., F. Chen, W. Wang, J. Dudhia, M. A. LeMone, K. Mitchell, M. Ek, G. Gayno, J. Wegiel, and R. H. Cuenca, 2004: Implementation and verification of the unified Noah land surface model in the WRF model. *20th Conference on Weather Analysis and Forecasting/16th Conference on Numerical Weather Prediction*, American Meteorological Society, Seattle, WA, US. [Available at http://meteora.ucsd.edu/cap/docs/tewari_et.al.pdf.]
- Tu, J.-Y., and C. Chou, 2013: Changes in precipitation frequency and intensity in the vicinity of Taiwan: Typhoon versus non-typhoon events. *Environ. Res. Lett.*, **8**, 014023, doi:10.1088/1748-9326/8/1/014023.
- von Storch, H., and F. W. Zwiers, 1999: *Statistical Analysis in Climate Research*. Cambridge University Press, 484 pp.
- Walsh, J. E., W. L. Chapman, V. Romanovsky, J. H. Christensen, and M. Stendel, 2008: Global climate model performance over Alaska and Greenland. *J. Climate*, **21**, 6156–6174.
- Wang, C.-C., G. T.-J. Chen, T.-C. Chen, and K. Tsuboki, 2005: A numerical study on the effects of Taiwan topography on a convective line during the mei-yu season. *Mon. Wea. Rev.*, **133**, 3217–3242.
- Wang, Z., and C.-P. Chang, 2012: A numerical study of the interaction between the large-scale monsoon circulation and orographic precipitation over South and

- Southeast Asia. *J. Climate*, **25**, 2440–2455.
- Wang, Z., L. Lin, X. Zhang, H. Zhang, L. Liu, and Y. Xu, 2017: Scenario dependence of future changes in climate extremes under 1.5°C and 2°C global warming. *Sci. Rep.*, **7**, 46432, doi:10.1038/srep46432.
- Wu, C.-C., T.-H. Yen, Y.-H. Huang, C.-K. Yu, and S.-G. Chen, 2016: Statistical characteristic of heavy rainfall associated with typhoons near Taiwan based on high-density automatic rain gauge data. *Bull. Amer. Meteor. Soc.*, **97**, 1363–1375.
- Yeh, H.-C., and G.-T. Chen, 2004: Case study of an unusually heavy rain event over eastern Taiwan during the mei-yu season. *Mon. Wea. Rev.*, **132**, 320–337.
- Zhao, M., I. M. Held, S.-J. Lin, and G. A. Vecchi, 2009: Simulations of global hurricane climatology, interannual variability, and response to global warming using a 50-km-resolution GCM. *J. Climate*, **22**, 6653–6678.